

Sliding Mode Measurement Feedback Control for Antilock Braking Systems

Cem Ünsal, *Member, IEEE*, and Pushkin Kachroo, *Member, IEEE*

Abstract—We describe a nonlinear observer-based design for control of vehicle traction that is important in providing safety and obtaining desired longitudinal vehicle motion. First, a robust sliding mode controller is designed to maintain the wheel slip at any given value. Simulations show that longitudinal traction controller is capable of controlling the vehicle with parameter deviations and disturbances. The direct state feedback is then replaced with nonlinear observers to estimate the vehicle velocity from the output of the system (i.e., wheel velocity). The nonlinear model of the system is shown locally observable. The effects and drawbacks of the extended Kalman filters and sliding observers are shown via simulations. The sliding observer is found promising while the extended Kalman filter is unsatisfactory due to unpredictable changes in the road conditions.

Index Terms—Adaptive control, nonlinear observers, state estimation, variable structure systems, wheel slip control.

I. INTRODUCTION

THE control of ground vehicle motions is becoming important due to recent research efforts on intelligent transportation systems, and especially, on automated highway systems [10], [8], [22]. In order to implement an advanced vehicle control system while obtaining desired vehicle motion, and providing safety, vehicle traction control should be realized. Traction control systems can be designed to satisfy various objectives of a single vehicle system or a platoon of closely spaced vehicles, such as assuring ride quality and passenger comfort.

Vehicle traction force directly depends on the friction coefficient between road and tire, which in turn depends on the wheel slip as well as road conditions. It is possible to influence traction force by varying the wheel slip, a nonlinear function of the wheel velocity and the vehicle velocity. A sliding mode controller to maintain the wheel slip at any given value is designed by Kachroo and Tomizuka [5]. This longitudinal traction controller is found to be giving better results than the conventional controllers are. On the other hand, a typical ABS system can only sense the angular wheel velocity and/or

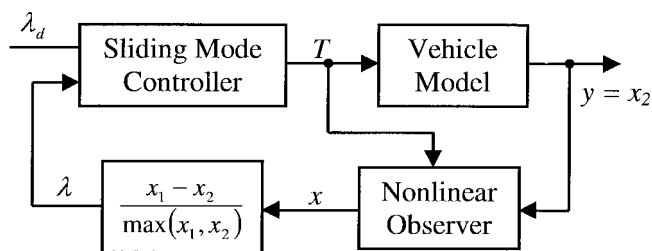


Fig. 1. The structure of the controller/observer system.

acceleration of the vehicle to estimate the wheel slip. Vehicle traction control can greatly improve the performance of vehicle motion and stability by providing anti-skid braking and anti-spin acceleration. The design of traction controller is based on the assumption that vehicle and wheel angular velocities are both available on-line by direct measurements and/or estimations. As angular wheel velocity is directly measured, only vehicle velocity is needed to estimate wheel slip. Two of the many methods for estimating the vehicle velocity are using magnetic markers imbedded in the pavement and the use of an accelerometer to calculate velocity by integration [8]. Both methods have drawbacks: one requires an accurate sensing system and infrastructure, the other frequent updates because of accumulation of integration errors.

In this paper, we will show that both wheel and vehicle speeds (states of the nonlinear system model) are observable from the output (wheel angular speed) for our vehicle and wheel dynamics model. Conventional ABS systems use velocity and acceleration data of the vehicle with a lookup table to calculate braking torque (or brake pressure) value. The aim of these controllers is to maintain the wheel slip at the peak of $[\mu - \lambda]$ curve (as discussed in Section II), but due to the qualitative design, that is not always guaranteed. We propose that an analytic design with full state feedback that will improve the performance of ABS; but we will try to obtain similar results using only partial state feedback. The overall system structure is given in Fig. 1.

A nonlinear observer will be designed to fit the requirements of the two dimensional system describing the vehicle dynamics. The verification of the design is done via simulation on Matlab/Simulink. The design of this observer will be a step toward the realization of more complex observers necessary for the headway control of vehicles with limited sensing (i.e., only the headway information).

Manuscript received October 29, 1996; revised May 27, 1998. Recommended by Associate Editor, R. Takahashi. This material is based upon work supported by VDOT and Virginia Tech's Center for Transportation Research under Smart Road Project.

C. Ünsal is with the Institute of Complex Engineering Systems, Carnegie Mellon University, Pittsburgh, PA 15261 USA.

P. Kachroo is with the Bradley Department of Electrical and Computer Engineering, Virginia Tech, Blacksburg, VA 24061-0111 USA.

Publisher Item Identifier S 1063-6536(99)01611-5.

TABLE I
WHEEL AND VEHICLE PARAMETERS

ω_w	Angular speed of the wheel
J_w	Moment of inertia of the wheel
T_e	Shaft torque from the engine
T_b	Brake torque
r_w	Radius of the wheel
F_t	Tractive force
F_w	Wheel viscous friction
N_v	Normal reaction force from the ground
ω_v	Angular speed of the vehicle
F_v	Wind drag force (function of vehicle velocity)
M_v	Vehicle mass
N_w	Number of driving wheels (acceleration) or the total number of wheels (braking).

In the next section, we introduce the system dynamics and resulting nonlinear differential equations. The use of sliding mode control for the system at hand, simulation results for the controller, discussion on the observability of the system and nonlinear observers will follow. Simulation results with observers in the feedback loop are given in Section VII. Appendix A includes the derivation of the limiting function for the sliding controller, while Appendix B details the necessary steps for checking the observability of the system.

II. SYSTEM DYNAMICS

In order to design a controller, a good representative model of the system is needed. In this section, we will describe the mathematical model for vehicle traction control. This model will then be used for system analysis, design of control laws and computer simulations. The model described in the paper, although relatively simple, retains the essential characteristics of the actual system. We will not discuss the stability of the system, but only state the necessary conditions.

Our model identifies the wheel speed and vehicle speed as state variables, and the torque applied to the wheel as the input. The state equations are the result of the application of Newton's law to wheel and vehicle dynamics. The dynamic equation for the angular motion of the wheel is given as

$$\omega_w^* = \frac{T_e - T_b - r_w(F_t + F_w)}{J_w}. \quad (1)$$

All the quantities in this equation are defined in Table I. The total torque consists of shaft torque from the engine, which is opposed by the break torque and the torque components due to tire tractive force and wheel friction force. The wheel viscous friction force developed on the tire-road contact surface depends on the wheel slip, which is defined as the difference between the vehicle and tire speeds, normalized by the maximum of these velocity values [vehicle speed for braking, wheel speed for acceleration; see (2)]. The engine torque and the effective moment of inertia of driving wheel depend on the transmission gearshifts.

Applying a driving torque or a braking torque to a pneumatic tire produces a tractive force at the tire-road contact patch [23]. The driving torque produces compression at the tire tread in front and within the contact patch. Consequently, the tire travels less distance than it would if it were free rolling.

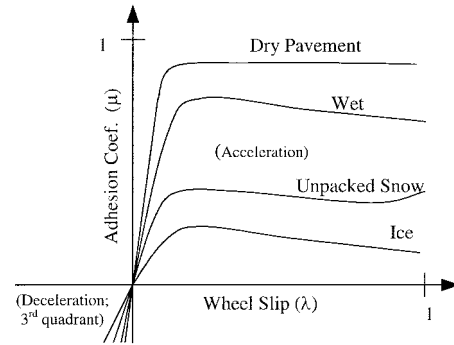


Fig. 2. Typical $\mu - \lambda$ curves for different road conditions.

Similarly, when a braking torque is applied, it produces a tension at the tire tread within the contact patch and at the front. Because of this tension, the tire travels more distance than it would during free rolling. This phenomenon is called the deformation slip or *wheel slip* [19], [23]. Mathematically, the wheel slip is defined as

$$\lambda = \frac{\omega_w - \omega_v}{\max\{\omega_w, \omega_v\}} \quad (2)$$

where ω_v is the vehicle angular velocity

$$\omega_v = \frac{V}{r_w} \quad (3)$$

which is equal to the linear vehicle velocity V divided by the radius of the wheel. The tractive force is given by

$$F_t = \mu(\lambda) \cdot N_v \quad (4)$$

where the normal tire reaction force N_v , depends on vehicle parameters such as the mass, location of the center of gravity, and the steering and suspension dynamics. The adhesion coefficient μ , which is the ratio between the tire tractive force and the normal road, depends on the tire-road conditions and the value of the wheel slip λ [3]. Fig. 2 shows a typical $\mu - \lambda$ curve [20]. A more mathematical description of the tire model is described by Peng and Tomizuka [13]. In our simulations, the function $\mu(\lambda) = (2\mu_p\lambda_p\lambda/\lambda_p^2 + \lambda^2)$ is used for a nominal curve, where μ_p and λ_p are the peak values. This function gives values compatible with experimental data given in the literature [23], especially in the range $\lambda \in [0, 0.3]$.

For various road conditions, the curves have different peak values and slopes. The adhesion coefficient—wheel slip characteristics are also influenced by operational parameters like speed and vertical load. The peak value for adhesion coefficient may have values between 0.1 (icy road) and 0.9 (dry asphalt and concrete; see Fig. 2).

The model for wheel dynamics is given in Fig. 3. The figure shows the parameters in Table I for acceleration case, for which tractive force and wheel friction are in the direction of motion. The wheel is rotating in clockwise direction, and slipping against the ground (i.e., $\omega_w > \omega_v$). The slipping produces the tractive force toward right causing the vehicle to accelerate. In the case of deceleration, the wheel still rotates in the clockwise direction, but skids against the ground (i.e., $\omega_w < \omega_v$). The skidding produces the tractive force toward left causing the vehicle to decelerate.

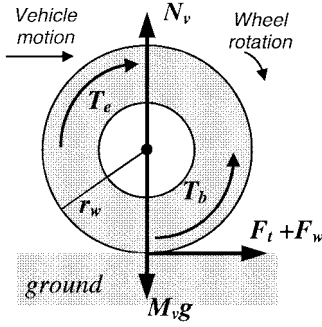


Fig. 3. Wheel dynamics.

The linear acceleration of the vehicle is governed by the tractive forces from the wheels and the aerodynamic friction force. The tractive force F_t is the average friction force of the driving wheels for acceleration and the average friction force of all wheels for deceleration. The dynamic equation for the vehicle motion is

$$\dot{V} = \frac{N_w F_t - F_v}{M_v}. \quad (5)$$

The linear acceleration of the vehicle is equal to the difference between the total tractive force available at the tire-road contact and the aerodynamic drag on the vehicle, divided by the mass of the vehicle. The total tractive force is equal to the product of the average friction force, F_t and the number of relevant wheels N_w . The aerodynamic drag is a nonlinear function of the vehicle velocity and is highly dependent on weather conditions. It is usually proportional to the square of the vehicle velocity.

A. Combined System and the Slip

The dynamic equation of the whole system can be written in state variable form by defining convenient state variables. We chose the state variables as the wheel and vehicle velocities

$$x_1 = \omega_w = \frac{V}{r_w} \quad x_2 = \omega_w. \quad (6)$$

Now, we can rewrite (1) and (5) as

$$\begin{aligned} \dot{x}_1 &= -f_1(x_1) + b_{1N} \cdot \mu(\lambda) \\ \dot{x}_2 &= -f_2(x_2) - b_{2N} \cdot \mu(\lambda) + b_3 \cdot T \end{aligned} \quad (7)$$

where

$$\begin{aligned} T &= T_e - T_b \\ f_1(x_1) &= \frac{F_v(f_w x_1)}{M_v r_w} \\ \lambda &= \frac{x_2 - x_1}{\max_i(x_i)} \\ b_{1N} &= \frac{N_v N_w}{M_v r_w} \\ f_2(x_2) &= \frac{F_w(x_2)}{J_w} \\ b_{2N} &= \frac{r_w N_v}{J_w} \quad b_3 = \frac{1}{J_w}. \end{aligned} \quad (8)$$

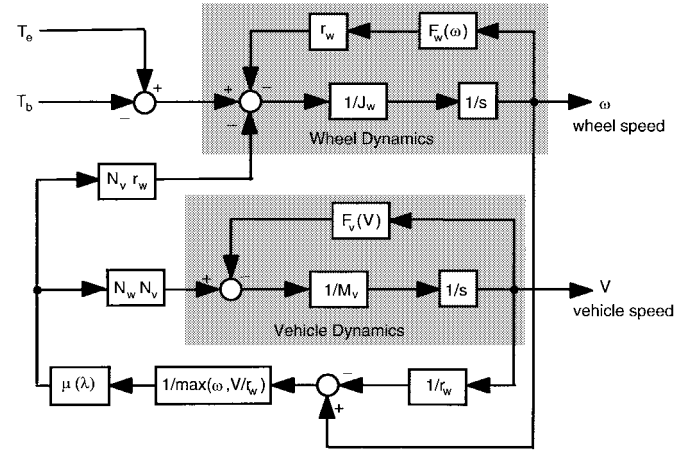


Fig. 4. Vehicle-Brake-road dynamics: One-wheel model.

The block diagram representation of the combined dynamic system is shown in Fig. 4. The control input is the applied torque at the wheels, which is equal to the difference between the shaft torque from the engine and the braking torque. During acceleration, engine torque is the primary input where as during deceleration it is the braking torque. The wheel slip is chosen here as the controlled variable for traction control algorithms because of its strong influence on the tractive force between the tire and the road.

We will first assume that wheel slip is calculated from (2) by using the measurements of wheel angular velocity and the estimated value of the vehicle velocity from either the accelerometer data or the magnetic marker data. Then, instead of the full state feedback, we will use a more realistic model output, where only the wheel velocity is measured, and insert a nonlinear estimator into the feedback loop (Fig. 1). By controlling the wheel slip, we control the tractive force to obtain the desired output, namely wheel and vehicle velocities, from the system. In order to control the slip, it is convenient to have the system dynamic equations in terms of the wheel slip. Since the functional relationship between the wheel slip and the state variables is different for acceleration and deceleration, we will only derive the equations for the deceleration case. The dynamic wheel slip equation for the acceleration case is also given, without derivations. During deceleration, the condition $x_2 < x_1$ is satisfied, and therefore the wheel slip is defined as

$$\lambda = \frac{x_2 - x_1}{x_1}. \quad (9)$$

Taking the time derivative, we obtain

$$\dot{\lambda} = \frac{\dot{x}_2 - (1 - \lambda) \cdot \dot{x}_1}{x_1}. \quad (10)$$

Substituting (7)–(9) into (10), we get (11), shown at the bottom of the next page. This gives the wheel slip equation for deceleration case. The equation is nonlinear and involves uncertainties in its parameters. The nonlinear characteristic equation is caused by the following factors.

- 1) The relationship of wheel slip with wheel velocity and vehicle velocity is nonlinear.
- 2) The $\mu - \lambda$ relationship is nonlinear.

- 3) There are multiplicative terms in the equation.
 4) Functions $f_1(x_1)$ and $f_2(x_2)$ are nonlinear.

In the case of acceleration, the equation is also nonlinear and involves uncertainties as shown in (12) at the bottom of the page. The local stability of the nonlinear system can be studied by linearizing the system around its equilibrium point. Kachroo and Tomizuka [4] stated that the system is stable in the deceleration case if the following condition is satisfied:

$$\frac{b_{1N}}{x_{20}} + b_{2N} \cdot \frac{x_{10}}{x_{20}^2} > \frac{\frac{df_1}{dx_1}(x_{10}) + \frac{df_2}{dx_2}(x_{20})}{\left| \frac{\partial \mu}{\partial \lambda} \right|}. \quad (13)$$

In the acceleration case, similar (but slightly different) conditions are obtained, using the eigenvalues of the Jacobian matrix for the nonlinear system.

III. SLIDING MODE CONTROL OF THE WHEEL SLIP

For wheel slip control, a nonlinear control strategy based on sliding mode is chosen. Sliding mode controllers are known to be robust to parametric uncertainties [17]. The following is the derivation of the sliding mode control law for wheel slip regulation. The slip dynamic equation for deceleration (11) can be written as

$$\dot{\lambda} = f + b \cdot u \quad (14)$$

where

$$f = \frac{(1 + \lambda) \cdot f_1(x_1) - f_2(x_2) - [b_{2N} + (1 + \lambda) \cdot b_{1N}] \cdot \mu(\lambda)}{x_1}$$

$$u = \frac{T}{x_1} \quad b = b_3. \quad (15)$$

Since the system is of first order, the switching surface $S(t)$ is defined by equating the sliding variable s , defined below, to zero

$$s(\lambda, t) \equiv \left(\frac{d}{dt} + \lambda \right)^{l-1} \cdot (\lambda - \lambda_d) = \lambda - \lambda_d \equiv \lambda_e \quad (16)$$

where λ_d denotes the desired slip, and λ_e is the error. The nonlinear function f is estimated as \hat{f} , and the estimation error on f is assumed to be bounded by some known function F , so that $|f - \hat{f}| \leq F$. (See Appendix A for the derivation of $F(x)$ for this particular application.) The control gain b is bounded as $0 \leq b_{\min} \leq b \leq b_{\max}$. The control gain b and its bounds can be time varying or state dependent. Since the control input is multiplied by the control gain in the dynamics, the geometric mean of the lower and upper bounds of the gain,

$\hat{b} = \sqrt{b_{\max} b_{\min}}$, is taken as the estimate of b . The controller is designed as

$$T = u \cdot x_1 \quad (17)$$

where

$$u = \hat{b}^{-1} \cdot [\hat{u} - k \operatorname{sgn}(s)] \quad \text{and} \quad (18)$$

$$\hat{u} = -\hat{f} - \dot{\lambda}_d. \quad (19)$$

A finite time is taken to reach the switching surface and the stability of the system is guaranteed with an exponential convergence once the switching surface is encountered, if the sliding gain k is chosen as

$$k \geq \alpha \cdot (F + \eta) + (\alpha - 1) \cdot |\hat{u}|. \quad (20)$$

The condition of gain k is direct result of the condition for the sliding variable outside of the switching surface $S(t)$

$$\frac{1}{2} \frac{d}{dt} s^2 \leq \eta |s| \quad (21)$$

that guarantees finite time to reach the surface if the initial tracking error is not zero. By integrating the condition above, and considering both negative and positive tracking errors, the following bound on the time interval to reach the surface is obtained [17]:

$$t_r \leq \frac{|s(t=0)|}{\eta}. \quad (22)$$

Switching control laws are known to be not practical to implement because of chattering. Chattering is caused by nonideal switching of the variable s around the switching surface. Delay in digital implementation causes s to pass to the other side of the surface $S(t)$, which in turn produces chattering. A practical approach for avoiding chattering is to introduce a region around $S(t)$ so that s changes its value continuously [5], [6]. A boundary layer of fixed width ϕ around the switching surface, and the function $isat(\cdot)$ is defined as

$$isat(a, b, s, \phi) = \begin{cases} \frac{as}{\phi} + \frac{b}{\phi} \int_0^t s dt, & \text{for } |s| < \phi \\ \operatorname{sgn}(s), & \text{otherwise.} \end{cases} \quad (23)$$

The parameters a and b are

$$a = \frac{2\gamma\phi}{k(\lambda_d)} \quad b = \frac{\gamma^2\phi}{k(\lambda_d)} \quad (24)$$

and the definition of the control input u is changed to

$$u = \hat{b}^{-1} \cdot [\hat{u} - k \cdot isat(a, b, s, \phi)]. \quad (25)$$

$$\dot{\lambda} = \frac{[(1 + \lambda) \cdot f_1(x_1) - f_2(x_2)] - [b_{2N} + (1 - \lambda) \cdot b_{1N}] \cdot \mu(\lambda) + b_3 T}{x_1} \quad (11)$$

$$\dot{\lambda} = \frac{[f_1(x_1) - (1 - \lambda) \cdot f_2(x_2)] - [(1 - \lambda) \cdot b_{2N} + b_{1N}] \cdot \mu(\lambda) + b_3 \cdot T}{x_2} \quad (12)$$

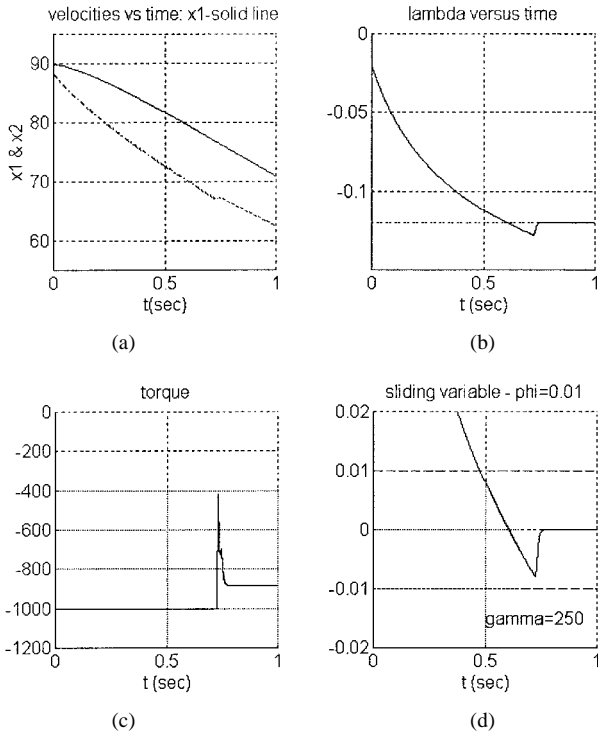


Fig. 5. Simulation results: (a) vehicle and wheel speeds, (b) wheel slip, (c) braking torque, and (d) sliding variable as functions of time.

The bandwidth of the filter for variable s is given by $[\gamma]$. Note that the second term in (25) acts as a PI controller in the region $s < |\phi|$. The first term, given by (19), attempts to cancel the nonlinear term in (14), and further adds the desired dynamics. If the cancellation of the nonlinear term is perfect, i.e., $f - (b/\hat{b}) \hat{f} \equiv 0$, (14), (19), (23), and (25) will result in a linear error equation with no forcing term, which implies that the slip error as well as the sliding variable s , all converge to zero. However, the cancellation can never be perfect, which can be easily understood by the presence of $\mu(\lambda)$ in (15). The integrator can absorb the error due to imperfect cancellation and assures superior performance.

IV. SIMULATION RESULTS WITH DIRECT STATE FEEDBACK

Fig. 5 shows the result of a simulation for which the initial and desired values of the wheel slip are -0.02 and -0.12 , respectively. In other words, the vehicle is already braking, but a better traction value is required. Maximum braking torque is limited at 1000 Nm. Also note that the peak value of the nominal curve used in the sliding mode controller is 0.7 , while the actual road conditions is simulated using a peak value of 0.8 .

The plot of the vehicle and wheel velocities in Fig. 5 indicates that the braking action causes the wheel slip to reach its desired value quickly. The average deceleration for the first second is approximately 0.56 g. As seen in the second figure, the time to reach the boundary layer is larger than the value given by $t_r \leq (|s(0)|/\eta) = (0.14/1.5) \approx 0.1$ s. This is due to the fact that the control input is limited. Furthermore, this example assumes no rate of change limitations on the applied brake. It is possible for the braking mechanism to introduce a

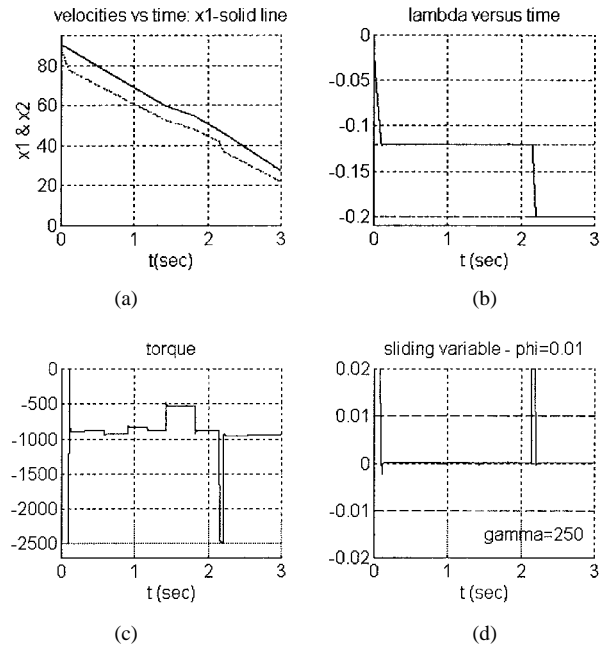


Fig. 6. Simulation results: (a) vehicle and wheel speeds, (b) wheel slip, (c) braking torque, and (d) sliding variable as functions of time.

delay to the applied torque, which would cause a longer time interval to reach the switching surface.

The function isat used in the boundary layer eliminates the chattering; the applied torque is smooth. The sliding variable reaches the boundary layer, and then approaches zero.

In the simulation example given in Fig. 6, the maximum torque value is increased. Thus, the time to reach the desired value of the wheel slip is distinctly less than the previous example. In this case, the desired wheel slip is reached in approximately 0.1 s. Fig. 6 also shows the effect of the change in the function parameters, road surface conditions and desired wheel slip. Between $t = 0.4$ s and $t = 1$ s, the value of the parameter b_{2N} is changed $\pm 10\%$. The applied torque is changed to compensate for these changes as seen in Fig. 6. The wheel slip (and the sliding variable) does not show any significant deviations. Around $t = 1.5$ s, we simulate a change in the road conditions: Peak value of the $\mu - \lambda$ curve is decreased from 0.8 to 0.5 . (The vehicle travels along an icy patch for approximately 0.5 s.) Again, the controller output is quickly changed to compensate, while the wheel slip is unaffected. Third, we increase the desired value of the slip around $t = 2.1$ s. The braking torque drastically increases to drive the variable s to the sliding surface, and the new value is reached again in less than 0.1 s.

V. OBSERVABILITY OF THE SYSTEM

To be able to use an estimator for the states of the dynamic model, we first have to prove that the states are observable from the output. The wheel angular speed that can be easily measured is defined as the output for the vehicle model we described in (7). Thus, the system equations become

$$\begin{aligned} \dot{x} &= f(x) + g(x) \cdot u \\ y &= h(x) \end{aligned} \tag{26}$$

where, from (7), the functions f, g, h are defined as

$$\begin{aligned} h(x) &= [0 \ 1] \cdot \begin{bmatrix} x_1 \\ x_2 \end{bmatrix} = x_2 \\ f(x) &= \begin{bmatrix} -f_1(x_1) + b_{1N} \cdot \mu(\lambda(x_1, x_2)) \\ -f_2(x_2) - b_{2N} \cdot \mu(\lambda(x_1, x_2)) \end{bmatrix} \quad g(x) = \begin{bmatrix} 0 \\ b_3 \end{bmatrix}. \end{aligned} \quad (27)$$

For the system given in (26), it has been proven that the system is *locally observable* at x_o if the dimension of the Jacobian of the observability vector, $\dim dO(x_o)$ is equal to n , where n is the dimension of the output set, and observability vector $O(x)$ is constructed with repeated time derivatives of the output vector [13]

$$O(x) = [y \ \hat{y} \ \ddot{y} \ \dots]^T. \quad (28)$$

It is important to note that, unlike linear systems, the rank condition, $\dim dO(x_o) = n$, guarantees only local observability. A good treatment of the subject can be found in [12]. Let us consider the first three rows of the observability matrix. Using the (27), we obtain

$$O^3(x) = [y \ \hat{y} \ \ddot{y}]^T = [x_2 \ \dot{x}_2 \ \ddot{x}_2] \quad (29a)$$

where x_2 and \dot{x}_2 are known, and the third term is calculated as follows:

$$\begin{aligned} \ddot{x}_2 &= -b_{2N} \cdot \frac{d\mu}{d\lambda} \cdot \frac{\partial \lambda}{\partial x_1} \cdot x_2 - \left(\frac{\partial f_2}{\partial x_2} + b_{2N} \cdot \frac{d\mu}{d\lambda} \cdot \frac{\partial \lambda}{\partial x_2} \right) \\ &\quad \cdot (-f_2(x_2) - b_{2N} \cdot \mu(\lambda) + b_3 \cdot T). \end{aligned} \quad (29b)$$

The Jacobian of the observability matrix $dO(x)$ is then (See Appendix B for the evaluation of the term A) shown in (30) at the bottom of the page. The Jacobian loses rank whenever the element (2,1) and A are *both* zero, and it is full rank otherwise. We show, in Appendix B, that these two terms are never zero at the same time. This proves that the system is *locally observable* everywhere. Therefore, it is possible to use a nonlinear observer to estimate the states of the system using only the output, i.e., the wheel speed.

VI. NONLINEAR OBSERVERS

Many researchers have worked on the development of state estimators for nonlinear and/or uncertain systems. Misawa and Hedrick [9] gave a state-of-the-art survey of the nonlinear observers. This work discusses several different methods including extended Kalman filter and sliding observers as well

as others. We use and compare extended Kalman filter and sliding observer for our state estimation, and briefly introduce these methods here.

A. Extended Kalman Filter

Kalman introduced the concept of an optimal linear filter in 1960 [7]. Kalman filter is known to minimize the mean square estimation error, and assumes that the dynamic system whose states are to be estimated can be described as a set of linear differential equations. A natural extension of this filter is *extended Kalman filter* [2], [18], which we choose as one of our observers. For a system model given as

$$\begin{aligned} \dot{x}(t) &= f(x(t), t) + w(t) \quad w(t) = N(0, Q(t)) \\ y(t) &= h(x(t), t) + v(t) \quad v(t) = N(0, R(t)) \end{aligned} \quad (31)$$

where $x \in \mathfrak{R}^n, w \in \mathfrak{R}^n, y \in \mathfrak{R}^m, v \in \mathfrak{R}^m, m \leq n$, and w and v are zero mean Gaussian noises with uncorrelated noise intensities Q and R , the initial conditions are assumed to be $x(0) = N(\hat{x}_0, P_0)$. For this system, the filter is given as

$$\begin{aligned} \dot{\hat{x}} &= f(\hat{x}(t), t) + K(t) \cdot [y(t) - h(\hat{x}(t), t)] \\ K(t) &= P(t) \cdot H^T(\hat{x}(t), t) \cdot R^{-1}(t) \\ \dot{P}(t) &= F(\hat{x}(t), t) \cdot P(t) + P(t) \cdot F^T(\hat{x}(t), t) + Q(t) \\ &\quad - P(t) \cdot H^T(\hat{x}(t), t) \cdot R^{-1}(t) \cdot H(\hat{x}(t), t) \cdot P(t) \end{aligned} \quad (32)$$

where F and H are the Jacobians of the functions f and h , respectively. Note that the functions F and H are evaluated at $x(t) = \hat{x}(t)$. From (8) and (27), we obtain (omitting the terms t for clarity)

$$\begin{aligned} F(\hat{x}(t)) &= \begin{bmatrix} -\frac{2c_v r_w x_1}{M_v} + b_{1N} \cdot \frac{d\mu}{d\lambda} \cdot \frac{\partial \lambda}{\partial x_1} & b_{1N} \cdot \frac{d\mu}{d\lambda} \cdot \frac{\partial \lambda}{\partial x} \\ -b_{2N} \cdot \frac{d\mu}{d\lambda} \cdot \frac{\partial \lambda}{\partial x_1} & -b_{2N} \cdot \frac{d\mu}{d\lambda} \cdot \frac{\partial \lambda}{\partial x_2} \end{bmatrix} \Bigg|_{x=\hat{x}} \\ H(\hat{x}(t)) &= [0 \ 1]. \end{aligned} \quad (33)$$

The correlation matrix elements P_i can be evaluated using (32). The extended Kalman filter is widely used. However, there are some drawbacks that make this filter nonfeasible for our application [9].

- P is only an approximation of the true covariance matrix and there is no *a priori* performance or stability guarantee. In our application, the values for the covariance matrix are stable.

$$dO^3(x) = \begin{bmatrix} 0 & 1 \\ b_{2N} \cdot \frac{d\mu}{d\lambda} \cdot \frac{\partial \lambda}{\partial x_1} & A \\ \frac{\partial}{\partial x_2} \{-f_2(x_2) - b_{2N} \cdot \mu(\lambda) + b_3 \cdot T\} & B \end{bmatrix} \quad (30)$$

- Comparing (31) and (32), we see that the perfect system knowledge is assumed. For this application, there is no way of knowing the operation point on the $\mu - \lambda$ curve, and therefore, the estimator uses the nominal values. However, the value of the adhesion coefficient calculated from the nominal curve may differ from the actual value, thus resulting in a modeling error.
- Evaluating F and H at $x = \hat{x}$ can introduce (even if f is the exact model) arbitrarily large errors.

B. Sliding Observers

Sliding observers are nonlinear state estimators based on the theory of variable structure systems [15], [21]. It was suggested by Slotine *et al.* [16]. For an n th order nonlinear system of the form $\dot{x} = f(x, t)$, $x \in \mathbb{R}^n$, and a vector of measurements that is linearly related to the state vector $y = Cx$, $y \in \mathbb{R}^m$, we define an observer of the following structure:

$$\dot{\hat{x}} = \hat{f}(\hat{x}, t) - HC(\hat{x} - x) - K1_s \quad (34)$$

where $\hat{x} \in \mathbb{R}^n$, \hat{f} is our model of f , H , and K are $n \times m$ gain matrices to be specified, and 1_s is an $m \times 1$ vector defined as

$$1_s = \begin{bmatrix} \text{sign}(\hat{y}_1) \\ \text{sign}(\hat{y}_2) \\ \vdots \end{bmatrix} \quad \text{or} \quad 1_s = \begin{bmatrix} \text{sat}(\hat{y}_1) \\ \text{sat}(\hat{y}_2) \end{bmatrix} \quad (35)$$

where $\hat{y}_i \equiv C \cdot (\hat{x} - x)$.

For our single measurement system, the observer equations are

$$\begin{bmatrix} \dot{\hat{x}}_1 \\ \dot{\hat{x}}_2 \end{bmatrix} = \begin{bmatrix} \hat{F}_1(\hat{x}_1, \hat{x}_2) \\ \hat{F}_2(\hat{x}_1, \hat{x}_2) \end{bmatrix} - \begin{bmatrix} h_1 \\ h_2 \end{bmatrix} \cdot [0 \ 1] \cdot \begin{bmatrix} \hat{x} - x_1 \\ \hat{x}_2 - x_2 \end{bmatrix} - \begin{bmatrix} k_1 \\ k_2 \end{bmatrix} \cdot \text{sign}(\hat{x}_2 - x_2) \quad (36)$$

where \hat{F}_i are estimates of the functions in (27), evaluated at the estimated points. When the sliding variable is chosen as being equal to the measurement error

$$s \equiv \tilde{y} = C \cdot (\hat{x} - x), \quad (37)$$

The sliding condition

$$s \cdot \dot{s} < 0 \quad (38)$$

on the sliding surface $s = 0$, will guarantee that the state observations will match the actual values. In our case, the sliding condition becomes

$$\tilde{x}_2 \cdot ((\hat{F}_2 - f_2 - b_3 \cdot u) - h_2 \cdot \tilde{x}_2 \cdot \text{sign}(\tilde{x}_2)) < 0 \quad (39)$$

where $\tilde{x}_i = \hat{x}_i - x_i$. The equivalent control method given by Utkin [21] provides the approximate sliding dynamics as

$$\dot{\tilde{x}} = (I - K(CK)^{-1}C) \cdot \Delta f \quad (40)$$

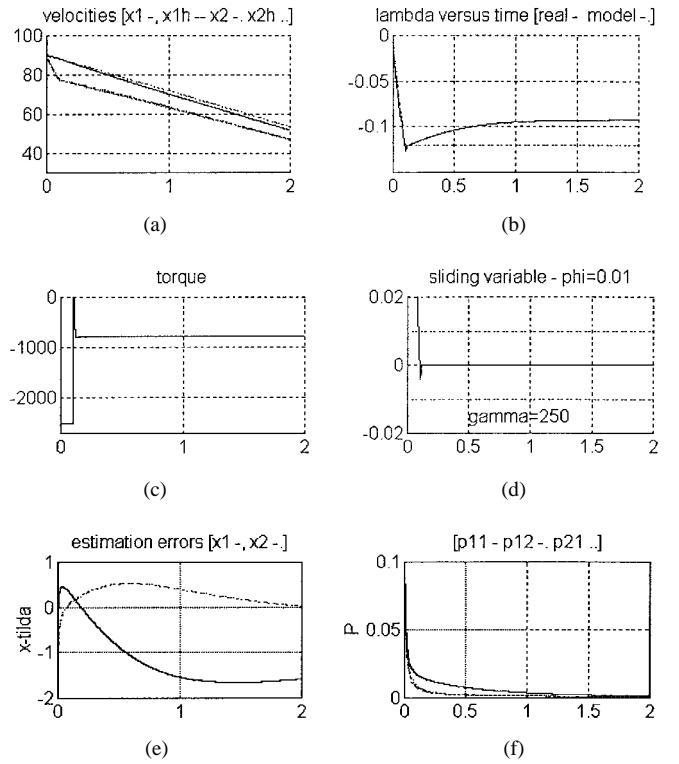


Fig. 7. Simulation results: (a) Vehicle and wheel speeds, (b) wheel slip, (c) braking torque, (d) sliding variable, (e) estimation errors, and (f) covariance matrix elements as functions of time.

where Δf_i are the error between the observer dynamics (36) and the actual system dynamics (27) as defined in (39). Using (40), we obtain the following:

$$\dot{\tilde{x}}_1 = \Delta f_1 - \frac{k_1}{k_2} \cdot \Delta f_2 \quad \dot{\tilde{x}}_2 = 0. \quad (41)$$

As seen from the (39)–(41) above, not much can be said about the gains h_i and k_i . The method for finding the gain matrices H and K for linear systems is given by Misawa and Hedrick [9]. However, the equations to be solved are based on the Jacobian of the function f , and thus, are very difficult to solve in our application. Furthermore, the indirect effects of the states on the wheel slip, and consequently, friction coefficient complicates the matter. Therefore, we choose the values of the four gain coefficients by trial-and-error. The values for the second state (wheel angular speed), which is the measurement from the system, are easily found for a stable response. The coefficients for the first state (vehicle angular speed) are more difficult to set.

VII. SIMULATION RESULTS WITH THE OBSERVERS

Fig. 7 shows the result of a simulation where the extended Kalman filter is used for state estimation. Since the system knowledge is not perfect, i.e., the evaluation of the adhesion coefficient is erroneous, the controller cannot drive the wheel slip to desired value. As seen in Fig. 7, when the peak values for the $\mu - \lambda$ curve are not the same for the actual model and the nonlinear estimator (0.8 and 0.7 for this example), the wheel slip cannot reach the desired value; there is a steady-state error. The estimation error in wheel velocity is driven to

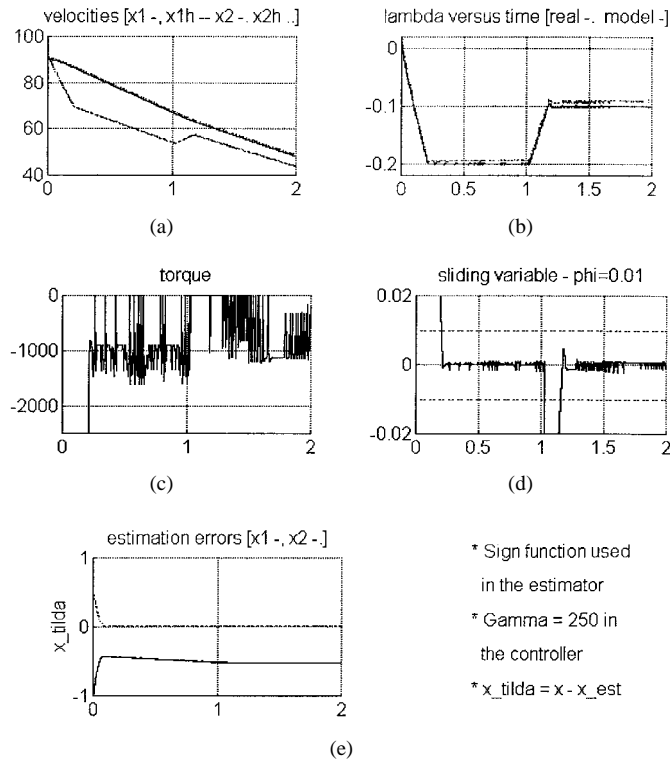


Fig. 8. Simulation results: (a) Vehicle and wheel speeds, (b) wheel slip, (c) braking torque, (d) sliding variable, and (e) estimation errors as functions of time.

zero due to the fact that wheel velocity is measured; however, the estimation of vehicle velocity has a steady-state error. Receiving only the estimated values from the observer, the sliding mode controller “thinks” that the wheel slip is at the desired value of -0.12 [Fig. 7(b)].

The performance of the extended Kalman filter for this application being unsatisfactory, the estimator is replaced by a sliding observer. Fig. 8 shows the result of a simulation with the sliding observer where desired value of the wheel slip is changed from -0.2 to -0.1 after 1 s. The gain coefficient for the observer is found by trial-and-error method. The chattering is due to the use of the saturation function $sat(s)$ that does not include the integral term. Replacing this function with the $isat(s)$ would eliminate the chattering, but the determination of (more) gain coefficients for the observer would make the initial design more difficult.

The performance of the sliding observer is satisfactory. The error is the wheel slip estimation (and the sliding variable) is minimal. Sliding observer is able to track vehicle speed (unobserved state) even though the initial estimates for the states are different than the actual values [Fig. 8(e)]. The response of the system to changes in the desired value of the wheel slip is comparable to the full-state feedback design. The steady-state error in the estimation of the first state is probably due to the choice of the gain coefficients for the matrices H and K .

VIII. CONCLUDING REMARKS

There are four main conclusions resulting from the work presented here. These are the following.

- Sliding mode controller based on mathematical design gives satisfactory results for this application of vehicle traction control. Desired wheel slip value for maximum deceleration can be achieved in minimum time, provided that the braking system is capable of producing the required torque.
- Since current ABS methods of measuring the vehicle speed are not perfect, an analytical observer may provide a better system performance. Furthermore, although the use of magnetic markers and magnetic strips for vehicle speed detection are shown to be feasible [11], the failure of these systems may lead to catastrophic collisions in an automated highway system. Therefore, an analytic observer based design for anti-lock braking system may prove to be very useful as a backup system.
- The performance of extended Kalman filter is poor, mainly due to the modeling errors, which we may not escape for applications in vehicle traction control.
- Sliding observer seems to be a good choice for this application, since it is shown to be robust against bounded modeling errors as described in Sections VI and VII. However, the complicated system model renders the analytic computation of gain matrices difficult.

Furthermore, the steady-state estimation error for nonlinear sliding observer is partially due to the error bounds defined for several parameters, as well as the definition of the $\mu - \lambda$ function estimate. A decrease in the estimation error range results in a relatively less estimation error in vehicle speed. Although the sliding controller and the observer are able to handle slight changes in the road surface conditions, the error bounds on the $\mu - \lambda$ function are not sufficient to compensate for significantly large changes in the road surface characteristics. Some form of information about the road surface may therefore improve the robustness of the wheel slip controller, since it will enable us to adjust the function estimation accordingly, and decrease the error range on the function estimation with the addition of this new information. Methods described in [14] can be used for road surface detection.

The local observability proof of the system is based on the simple dynamic model we assumed, and the functional representation of the $\mu - \lambda$ curve. Changes in the system model and in the function description will obviously affect the proof of observability. However, we believe that the longitudinal model we employed is representative of the vehicle characteristics as long as the lateral movement of the vehicle can be neglected. In addition, the functional representation of the adhesion coefficient is a good representation of the wheel characteristics, especially for the range the wheel slip controller would operate.

The work presented in this paper will be continued in the future. Our research is directed toward the analytical determination of the gain matrices for the sliding observer. If we can determine the gain coefficients analytically so that the error dynamics is stable, then our method of controlling vehicle traction for antilock braking may be a better solution to the optimal braking problem, and a safety alternative for AHS applications. Furthermore, the local observability condition for

where, again neglecting $f_2(x_2)$, A is calculated as

$$\begin{aligned}
 A = \frac{\partial \dot{y}}{\partial x_1} = & -b_{2N} \cdot \left(\frac{d^2 \mu}{d\lambda^2} \cdot \frac{\partial \lambda}{\partial x_1} + \frac{d\mu}{d\lambda} \cdot \frac{\partial^2 \lambda}{\partial x_1^2} \right) \cdot x_2 \\
 & - \left(b_{2N} \cdot \frac{d\mu}{d\lambda} \cdot \frac{\partial \lambda}{\partial x_1} \right) \cdot \frac{\partial x_2}{\partial x_2} \\
 & - b_{2N} \cdot \left(\frac{d^2 \mu}{d\lambda^2} \cdot \frac{\partial \lambda}{\partial x_1} \cdot \frac{\partial \lambda}{\partial x_2} + \frac{d\mu}{d\lambda} \cdot \frac{\partial^2 \lambda}{\partial x_1 \partial x_2} \right) \\
 & \cdot (-b_{2N} \cdot \mu + b_3 \cdot T) \\
 & - \left(b_{2N} \cdot \frac{d\mu}{d\lambda} \cdot \frac{\partial \lambda}{\partial x_2} \right) \cdot \left(-b_{2N} \cdot \frac{d\mu}{d\lambda} \cdot \frac{\partial \lambda}{\partial x_1} + b_3 \cdot \frac{\partial T}{\partial x_1} \right). \tag{B3}
 \end{aligned}$$

Element (2,1) of the Jacobian of the observability matrix is zero whenever $(d\mu/d\lambda) = 0$, i.e., at the peak of the $\mu - \lambda$ curve. Otherwise, the rank of the matrix is two and the system is observable. Furthermore, at the peak of the $\mu - \lambda$ curve, the element (3,1) of the matrix, namely A , can be evaluated as follows. Since $(\partial x_3/\partial x_1) = 0$, some of the terms in (B3) drop and we are left with

$$\begin{aligned}
 A = \frac{\partial \dot{y}}{\partial x_1} = & -b_{2N} \cdot \frac{d^2 \mu}{d\lambda^2} \cdot \frac{\partial \lambda}{\partial x_1} \cdot x_2 \\
 & - b_{2N} \cdot \frac{d^2 \mu}{d\lambda^2} \cdot \frac{\partial \lambda}{\partial x_1} \cdot \frac{\partial \lambda}{\partial x_2} \cdot (-b_{2N} \mu(\lambda) + b_3 \cdot T) \\
 = & -b_{2N} \cdot \frac{d^2 \mu}{d\lambda^2} \cdot \frac{\partial \lambda}{\partial x_1} \\
 & \cdot \left(x_2 + \frac{\partial \lambda}{\partial x_3} \cdot (-b_{2N} \cdot \mu(\lambda) + b_3 \cdot T) \right). \tag{B4}
 \end{aligned}$$

In this term, the parameter b_{2N} , partial derivative $\partial \lambda/\partial x_1$ [according to (9)], and the second derivative $d^2 \mu/d\lambda^2$ are non zero. For our definition of the $\mu - \lambda$ function, this can be seen easily

$$\begin{aligned}
 \mu(\lambda) = \frac{2\mu_p \lambda_p \lambda}{\lambda_p^2 + \lambda^2} & \equiv \frac{a\lambda}{b + \lambda^2} \Rightarrow \frac{d\mu}{d\lambda} = \frac{a(b - \lambda^2)}{(b + \lambda^2)^2} \Rightarrow \frac{d^2 \mu}{d\lambda^2} \\
 & = \frac{-2a\lambda(b + \lambda^2) \cdot [(b + \lambda^2) + 2(b - \lambda^2)]}{(b + \lambda^2)^4}. \tag{B5}
 \end{aligned}$$

Therefore, the second derivative of μ is zero if and only if

$$(b + \lambda^2) + 2(b - \lambda^2) = 3b - \lambda^2 = 0 \quad \text{or} \quad \lambda = \pm \lambda_p \sqrt{3}. \tag{B6}$$

This condition is also satisfied since the point where $(d\mu/d\lambda) = 0$ is the peak, and the second derivative cannot be zero to satisfy the local minimum (or maximum for acceleration case) condition. Therefore, if we can prove that the sum below [i.e., third term in A ; see (B4)] is not zero at the peak, then we would guarantee the rank condition necessary for the observability of the system, since we would prove that the term A is not zero whenever element (2,1) of the Jacobian is

$$\begin{aligned}
 x_2 + \frac{\partial \lambda}{\partial x_2} (-b_{2N} \mu(\lambda) + b_3 T) = 0 & \Leftrightarrow T \\
 = \frac{1}{b_3} (-x_2 x_1 + b_{2N} \mu(\lambda)). \tag{B7}
 \end{aligned}$$

Thus, the system is *not* locally observable only if we operate at the peak of the $\mu - \lambda$ curve, *and* the input is kept at a constant value given in (B7). Obviously, this is a very rare case. Even if this situation occurs, the error in the state estimation will grow and the input torque value will immediately change. Also note that we only considered an observability vector is size three here. It may be possible to meet the rank condition by considering higher derivatives of the output y .

ACKNOWLEDGMENT

The authors would like to thank anonymous reviewers for their constructive comments. First author would also like to thank Dr. D. K. Lindner of the Bradley Department of Electrical and Computer Engineering at Virginia Tech for his valuable guidance.

REFERENCES

- [1] H. H. Braess, "Prometheus, contribution to a comprehensive concept for future road traffic," *Smart Vehicles*. Lisse, The Netherlands: Swets and Zeitlinger, 1995, pp. 3–36.
- [2] A. Gelb, *Applied Optimal Estimation*. Cambridge, MA: MIT Press, 1974.
- [3] J. L. Harned *et al.*, "Measurement of tire break force characteristics as related to wheel slip control system design," *SAE Trans.*, vol. 78, no. 690214, pp. 909–925, 1969.
- [4] P. Kachroo and M. Tomizuka, "Vehicle traction control and its applications," Univ. California, Berkeley, Inst. Transportation, Tech. Rep. UIPRR-94-08, 1994.
- [5] —, "Sliding mode control with chattering reduction and error convergence for a class of discrete nonlinear systems with application to vehicle control," *ASME Int. Mech. Eng. Congr. Expo*, San Francisco, CA, 1995.
- [6] —, "Chattering reduction and error convergence in the sliding mode control of a class of nonlinear systems," *IEEE Trans. Automat. Contr.*, vol. 41, July 1996.
- [7] R. E. Kalman, "On a new approach to filtering and prediction problems," *ASME J. Basic Eng.*, vol. 28, Mar. 1960.
- [8] T. L. Lasky and B. Ravani, "A review of research related to automated highway system (AHS)," Univ. California, Davis, Interim Rep. FHWA, Contract DTFH61-93-C-00189, Oct. 25, 1993.
- [9] E. A. Misawa and J. K. Hedrick, "Nonlinear observers—A state-of-the-art survey," *ASME J. Dynamic Syst., Meas., Contr.*, vol. 111, pp. 344–352, 1989.
- [10] National Automated Highway System Consortium, Nov. 20, 1997. Available <http://nahsc.volpe.dot.gov/ahs/>
- [11] —, "Technical feasibility demonstration, Aug. 1997." Available <http://monolith-mis.com/ahs>.
- [12] H. Nijmeijer and A. J. van der Shaft, *Nonlinear Dynamical Control Systems*. New York: Springer-Verlag, 1990.
- [13] H. Peng and M. Tomizuka, "Vehicle lateral control for highway automation," *Proc. Amer. Contr. Conf.*, San Diego, CA, 1990, pp. 788–794.
- [14] Y. Shinmoto J. Takagi, K. Egawa, Y. Murata, and M. Takeuchi, "Road surface recognition sensor using an optical spatial filter," *IEEE Conf. ITS*, Boston, MA, Nov. 1997.
- [15] J.-J. E. Slotine, "Sliding controller design for nonlinear systems," *Int. J. Contr.*, vol. 84, 1984.
- [16] J.-J. E. Slotine, J. K. Hedrick, and E. A. Misawa, "On sliding observers for nonlinear systems," *ASME J. Dynamic Syst., Meas. Contr.*, vol. 109, pp. 245–252, Sept. 1989.
- [17] J.-J. E. Slotine and W. Li, *Applied Nonlinear Control*, Chapter 7. Englewood, CA: Prentice-Hall, 1991.
- [18] H. W. Sorenson, Ed., *Kalman Filtering: Theory and Applications*. New York: IEEE Press, 1985.
- [19] J. J. Taborek, *Mechanics of Vehicle*. Cleveland, OH: Penton, 1957.
- [20] H. S. Tan and M. Tomizuka, "An adaptive sliding mode vehicle traction controller design," in *Proc. Amer. Contr. Conf.*, vol. 2, pp. 1856–1861, 1990.
- [21] V. I. Utkin, *Sliding Modes and Their Application in Variable Structure System*. Moscow, USSR: MIR, 1978.
- [22] P. Varaiya, "Smart cars on smart roads: Problems of control," *IEEE Trans. Automat. Contr.*, vol. 38, pp. 195–207, Feb. 1993.
- [23] J. Y. Wong, *Theory of Ground Vehicles*. New York: Wiley, 1978.

Cem Ünsal (S'92–M'93) received the B.S. degree in electrical engineering from Bogazici University, Istanbul, Turkey, in 1991, and the M.S. and Ph.D. degrees in electrical engineering from Virginia Polytechnic Institute and State University (Virginia Tech), Blacksburg, VA, in 1993 and 1997, respectively.

He is currently working as a Postdoctoral Fellow at the Institute for Complex Engineered Systems (ICES), Carnegie Mellon University, Pittsburgh, PA. His current research interests include modular robotics, distributed control, planning, and nonlinear observers.

Dr. Ünsal is a member of ASEE.

Pushkin Kachroo (S'89–M'90) received the B.Tech. degree from the Indian Institute of Technology at Bombay in 1988, the M.S. degree from Rice University, Houston, TX, in 1990, and the Ph.D. degree from the University of California at Berkeley in 1993.

He was a Research Scientist at the Center for Transportation Research at the same university for three years. Prior to that, he was a Research Engineer at the R&D laboratory of the Lincoln Electric Company working in their robotics program to develop their laser vision-based robotic welding system. He is currently an Assistant Professor of the Bradley Department of Electrical and Computer Engineering at Virginia Tech. His research interests include theory, application, and microprocessor implementations of nonlinear feedback control systems, such as in transportation and communication systems. He is currently authoring two books: *Incident Management* and *Feedback Control for Dynamic Traffic Assignment*, to be published by Artech House by the end of 1999.

Dr. Kachroo has a P.E. certification from the State of Ohio.